GEOPHYSICS, VOL. 72, NO. 3 (MAY-JUNE 2007); P. B47–B57, 16 FIGS., 2 TABLES.
10.1190/1.2539353

Case History

Hydrogeologic assessment of the Amchitka Island nuclear test site (Alaska) with magnetotellurics

Martyn Unsworth[1], Wolfgang Soyer[2], Volkan Tuncer[1], Anna Wagner[3], and David Barnes[3]

ABSTRACT

Amchitka Island, in Alaska, was used for underground nuclear testing from 1965 to 1971. Since the test program concluded, there have been concerns about the possible release of radionuclides into the marine environment of the Aleutian Islands. The hydrogeology of islands such as Amchitka is characterized by a layer of freshwater overlying a saltwater layer, with the salinity increasing across a transition zone (TZ). Hydrogeologic modeling can provide an estimate of the timing and amount of radionuclide release from the explosions beneath Amchitka Island. This modeling is inconclusive because of a lack of information regarding subsurface structure. To address this problem, magnetotelluric (MT) data were collected on Amchitka Island in 2004. Broadband MT data were recorded on profiles passing through three explosion sites to give information about subsurface porosity and salinity. A 2D MT inversion produced models of subsurface electrical resistivity and showed a pattern of increasing, decreasing, and increasing resistivity with depth at each test site. The depth at which resistivity begins to decrease defines the top of the TZ. The deeper increase in resistivity approximates the base of the TZ. The depths of the top and bottom of the TZ were determined as follows: Cannikin 900–2500 m; Long Shot 600–1700 m; Milrow 900–1700 m. Uncertainties were estimated for these depths. Effective porosities were also estimated and ranged from 10%–20% at the surface to 1%–3% at 3-km depth. These porosities are higher than those assumed in several hydrogeologic models, and give longer transit times from the explosion to the marine environment. Subject to the limits of the analysis, it appears that each of the cavities resulting from underground nuclear explosions is located in the TZ from fresh to saltwater. This implies shorter transit times to the marine environment than if the detonations had been located in the saltwater layer.

INTRODUCTION

From 1965 to 1971, Amchitka Island in the western Aleutian Islands of Alaska was used as an underground test site for nuclear weapons that were too large for the Nevada test site. Projects Long Shot, Milrow, and Cannikin tested nuclear warheads with yields of approximately 80, 1000, and 5000 kilotons, respectively. Since the test program was concluded, there have been concerns about the release of radionuclides into the marine environment. The hydrogeology of an island such as Amchitka is characterized by a freshwater layer that is recharged from precipitation, and discharges offshore. Groundwater flow in the freshwater layer can be quite rapid, while the underlying saltwater layer is relatively stagnant (Hubbert, 1940; Freeze and Cherry, 1979). It is vital to understand the hydrogeologic context of the nuclear explosions on Amchitka Island, because this controls the timing of radionuclide transport into the marine environment, which is a major concern for both native groups and commercial fisheries.

A number of hydrogeologic studies were made prior to the test program (U.S. Army Corps of Engineers, 1965). Groundwater modeling has been used to estimate transit times from the explosion cavities to the ocean and, without geophysical constraints, gave a wide

Manuscript received by the Editor June 29, 2006; revised manuscript received November 6, 2006; published online March 26, 2007.
[1]University of Alberta, Department of Physics, Edmonton, Alberta, Canada. E-mail: unsworth@phys.ualberta.ca; vtuncer@phys.ualberta.ca.
[2]Formerly University of Alberta, Department of Physics, Edmonton, Alberta, Canada; presently Geosystem SRL, Via Clericetti, Milano, Italy. E-mail: wsoyer@geosystem.net
[3]University of Alaska, Water and Environmental Research Center, Civil and Environmental Engineering Department, Fairbanks, Alaska. E-mail: ftamf@uaf.edu; ffdlb@uaf.edu.

range of times (Wheatcraft, 1995; Hassan et al., 2002). Since 1995, there has been a concerted effort to evaluate and remediate sites in the United States that were contaminated during the production and testing of nuclear weapons. Some of this work has been undertaken through the Consortium for Risk Evaluation with Stakeholder Participation (CRESP). In 2004, a CRESP expedition visited Amchitka Island and undertook a multidisciplinary evaluation of the environment. A key component of this research was an onshore magnetotelluric (MT) survey that investigated the subsurface porosity and salinity structure. In this paper, the MT data are described, and the interpretation is outlined. Finally, a hydrogeologic modeling study is described that uses the MT data as a key constraint.

BACKGROUND AND PREVIOUS STUDIES

Geologic setting

Amchitka Island is located in the forearc of the Aleutian subduction zone. The bedrock is primarily volcaniclastic rocks of Tertiary age with both lava flows and intrusive units (U.S. Army Corps of Engineers, 1965). Tectonic processes in the rapidly deforming forearc have produced a series of faults oriented northeast-southwest. A number of wells were drilled and cored, and resistivity logs were measured at the Long Shot site in 1964 (U.S. Army Corps of Engineers, 1965). The Long Shot explosion was located within an andesite sill within the Banjo Point formation, which consists mainly of basaltic rocks of submarine deposition (Carr and Quinlivan, 1969). Deep wells were also drilled at the Milrow and Cannikin test sites and revealed similar geology to a depth of 2 km.

Coastal hydrogeology

The hydrogeology at many coastal locations is characterized by a layer of freshwater that is replenished from rain, and which overlies a deeper saltwater layer intruding from the ocean. The change from fresh to saltwater typically takes place over a broad transition zone (TZ) whose geometry is the result of a dynamic balance between buoyancy and diffusive effects. The wells drilled on Amchitka Island prior to nuclear testing gave some indications of the depth of the TZ but were not adequate to constrain hydrogeologic models. Geophysical imaging can be used to study this scenario through remote sensing of the electrical resistivity.

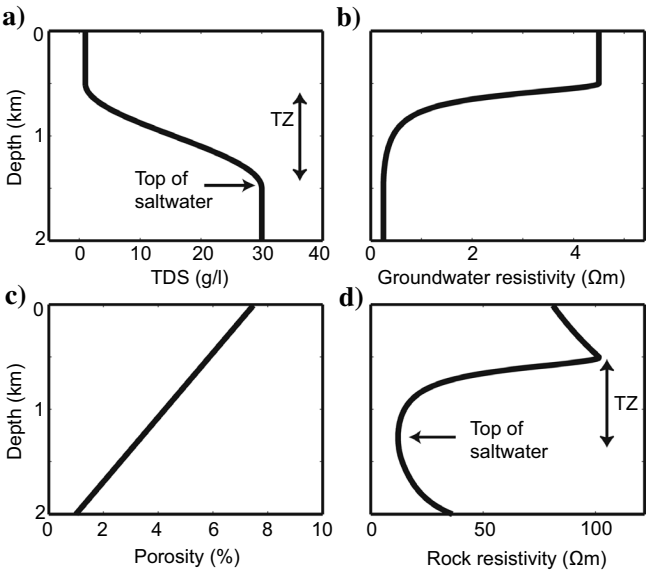

Figure 1. Theoretical study of the effect of subsurface porosity and salinity on the resistivity of a rock. (a) Salinity as a function of depth (TDS = total dissolved solids), (b) resistivity of the groundwater, (c) porosity decreases with depth, and (d) the rock resistivity decreases through the TZ, and increases in the saltwater layer. TZ = transition zone from fresh to saltwater.

The bulk resistivity in the near surface is controlled by the salinity of the groundwater, the porosity, and the degree of interconnection of the fluid (Ward, 1990). Figure 1a shows the salinity-depth profile for a typical coastal location with a transition from fresh to saltwater. The groundwater resistivity, computed with the empirical equation of Block (2001), decreases through the TZ as the salinity increases (Figure 1b). Porosity typically decreases with depth (Rubey and Hubbert, 1959; Giles et al., 1998), and a simple linear variation is shown in Figure 1c. Combining the information in Figure 1b and c, and assuming a relatively high degree of interconnection between the pores, the bulk resistivity of the rock was computed using Archie's Law (Archie, 1942) (Figure 1d). The TZ is expressed as a decrease of bulk resistivity with increasing depth. This is because between depths of 500 and 1200 m the resistivity decreases as the groundwater becomes more saline. Below 1200-m depth, the salinity is constant, and the decreasing porosity caused by increasing overburden pressure causes a rise in bulk resistivity. The top of the saltwater thus corresponds to the depth at which the bulk resistivity begins to increase again with depth. This study suggests that under favorable conditions, electromagnetic (EM) surveys can determine the subsurface fluid distribution and composition in a noninvasive manner. Note that the porosity value used in computations of bulk resistivity will be the effective porosity. This is less than the actual porosity, since only well-connected pores will make a major contribution to the transport of electric current or the flow of groundwater.

A number of geophysical techniques can be used to measure the near-surface electrical resistivity (McNeill, 1990). Direct current resistivity and ground-based loop-loop EM surveys can be used for shallow studies (Hagemeyer and Stewart, 1990; Goldstein et al., 1990). For deeper penetration, the time-domain method can image to depths in excess of 1 km by using a larger transmitter loop (Hoekstra and Blohm, 1990). For imaging at greater depths, the MT technique is most effective and uses natural EM signals in the band 1000–0.001 Hz. In audio-frequency magnetotellurics (AMT), frequencies of 10,000–10 Hz are used. If the natural signals are not adequate, then they can be supplemented by the use of a transmitter in the controlled-source audio-magnetotelluric (CSAMT) method (Unsworth et al., 2000). The target depths of 1–2 km on Amchitka were too deep for DC resistivity and at the depth limit for large loop time-domain methods. The logistical effort for large loop time-domain measurements would have been significant in the trackless tundra, so MT exploration was chosen as the most effective tool for mapping the salinity and porosity beneath the island. In addition, it was also hoped that the MT survey would detect subsurface features associated with underground nuclear explosions. Zones of fracturing, such as the shot cavity and collapse chimney, would be expected to have a lower resistivity, because of the enhanced porosity. It was also expected that faults might be detected through their effects on groundwater flow. Faults can act as both seals that prevent groundwater flow or conduits with enhanced porosity and hydraulic conductivity (Caine et al., 1996; Unsworth et al., 1997; Unsworth et al.,

2000). Hydrogeologic models are very sensitive to the presence of shallow faults, and locating major zones of enhanced flow is vital for accurate modeling.

DATA COLLECTION AND ANALYSIS

MT data collection

Broadband MT data were collected at 29 stations on Amchitka Island in June 2004, using six Phoenix Geophysics V5-2000 systems (Figure 2). Details of data acquisition are listed in Unsworth et al. (2005). Where logistically possible, both electric and magnetic field data were recorded. At sites far from roads, only electric field data were recorded, and the magnetic fields from the nearest five-channel station were used in the data processing. Magnetic fields generally exhibit a weaker spatial variation than the electric fields, and this assumption was shown to be valid by Unsworth et al. (2005) for the Amchitka Island data.

Time-series analysis

Time series were processed using the algorithm of Egbert and Booker (1986). Strong winds caused significant ground motion throughout the survey and resulted in magnetic noise that caused a downward bias in the apparent resistivity (Figure 3a). This noise was removed through use of the remote-reference technique (Gamble et al., 1979) with a station separation of a few hundred meters (Figure 3b). Six MT units recorded simultaneously, giving data that were used for multistation data processing (Egbert, 1997). At some stations, this gave a modest improvement over the remote-reference results. Vertical magnetic fields were also recorded during the survey, but even with remote-reference processing, it was not possible to obtain usable data.

Dimensionality of the MT data

Before MT data can be converted into a resistivity model of the subsurface, it is essential to understand the dimensionality of the data. Given the lateral contrast in resistivity produced by the seawater, a 1D approach is not valid. A 2D analysis is much simpler than a full 3D analysis, but must be carefully justified. The geoelectric strike direction was computed using the phase-tensor method (Caldwell et al., 2004) (Figure 4). As the frequency decreases, the depth sampled by the MT signals increases. At high frequency (1000–10 Hz), the strike direction is poorly defined, and the MT data are approximately 1D. At frequencies below 10 Hz, a well-defined strike of N55°W or N35°E is observed. Note that there is a 90° ambiguity in the strike angle and external information must be used to determine which of these directions is correct. Since the geometry of the low-resistivity seawater dominates the resistivity structure, it is clear that an island parallel strike of N55°W is appropriate. The MT data were rotated to this coordinate system for all subsequent analysis.

MT pseudosections, apparent resistivity, and phase curves

A typical apparent resistivity and phase curve on the Long Shot profile are shown in Figure 3b. The electric currents flowing along the island comprise the transverse-electric (TE) mode, and electric current flowing across the island comprise the transverse-magnetic (TM) mode. In a 1D configuration, these two modes give identical values of apparent resistivity and phase. However, over a 2D earth, the apparent-resistivity values computed from the TE and TM modes will be different. Since the depth of MT signal penetration increases as frequency decreases, the horizontal axis can be considered as a proxy for depth. At high frequency (shallow depth), the apparent resistivity is approximately constant at a value of 30 Ωm. Be-

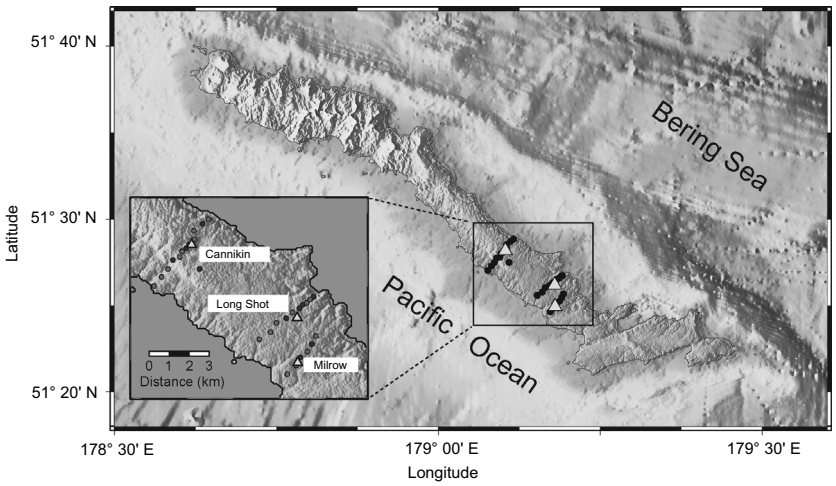

Figure 2. Map of Amchitka Island showing the MT transects and bathymetry. The triangles denote the locations of the nuclear explosions. Black circles show the locations at which MT data were recorded in June 2004. Inset shows details with 2E stations (black dots) and five-channel stations (gray dots).

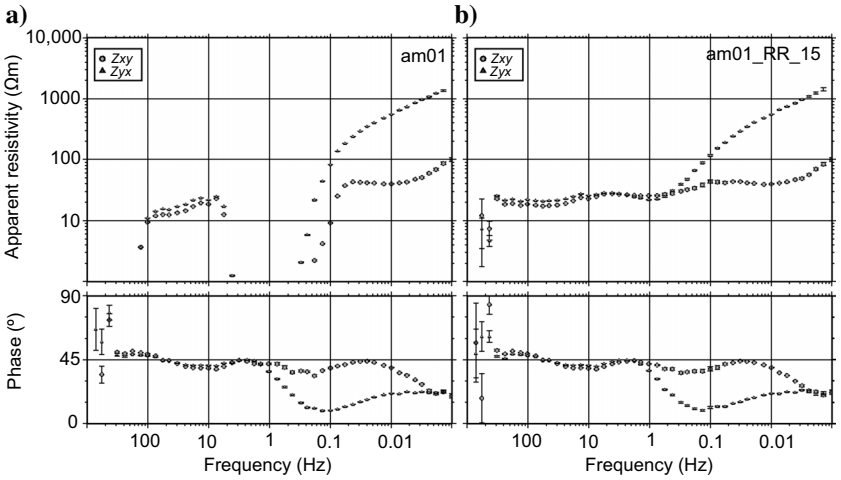

Figure 3. Apparent resistivity and phase recorded at station AM01. (a) Local processing showing the effect of severe down bias from 10–0.1 Hz, (b) remote-reference processing essentially removes the bias. Array processing with stations AM15, AM21, AM20, and AM18 yielded comparable results to (b). Note that *xy* = transverse-electric (TE) mode and *yx* = transverse-magnetic (TM) mode.

low 1 Hz, the TE and TM curves diverge. The TM-mode curve shows high apparent resistivities, while the TE-mode curve exhibits lower values. This basic pattern is observed at all MT sites and is caused by the effect of the ocean: The low resistivity ocean layer increases the TM-mode electric currents that flow across the island. The apparent resistivity is the ratio of electric-field to magnetic-field strengths, and this increases the apparent resistivity.

The MT data on each profile can also be displayed in pseudosection format with distance on the horizontal axis and frequency on the vertical axis. Because lower frequencies penetrate deeper into the earth, this gives an impression of how resistivity varies with depth. The Long Shot pseudosection displays a pattern of low-high-low-high apparent resistivity in both TE-mode apparent resistivity and phase (labeled C-R-C-R in Figure 5). A pattern of conductive 300–100 Hz), resistive (30–10 Hz), conductive (3–0.3 Hz), and resistive (0.1–0.03 Hz) features is observed in Figure 3. The MT phase also exhibits these changes, since a phase angle above 45° is considered high and indicates a conductive structure, while a phase below 45° indicates resistive structure. These subtle oscillations in apparent resistivity and phase are the result of an approximately layered resistivity structure in the upper 1–2 km of the subsurface. Note also that the TM-mode pseudosections show the high resistivity and low phase of the ocean effect below a frequency of 0.1 Hz. This obscures the oscillations caused by the layered structure in the upper 1–2 km of the island. The relatively smooth variation in apparent resistivity across the island on each profile indicates a smooth spatial variation in subsurface resistivity. The Milrow pseudosection was similar to the Long Shot line and is not shown in this paper. The pseudosection was noisier than the other profiles because recording times were reduced — less than 6 hr at some stations.

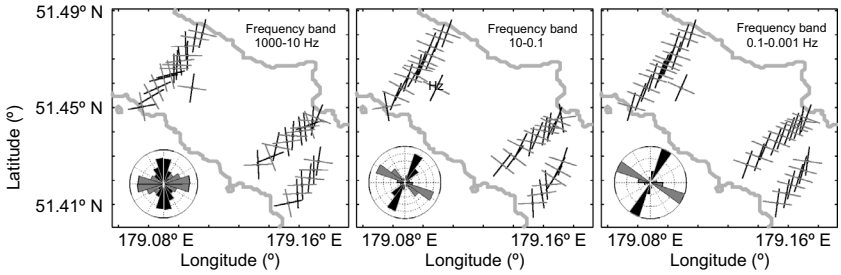

Figure 4. Dimensionality analysis. The gray and black lines denote the geoelectric strike direction that gives the best fit to the measured 2D data. Note that there is a 90° ambiguity in this quantity. At high frequencies (1000–10 Hz), the strike direction is poorly determined. At lower frequencies, corresponding to deeper signal penetration, a well-defined strike, parallel to the axis of the island, is observed.

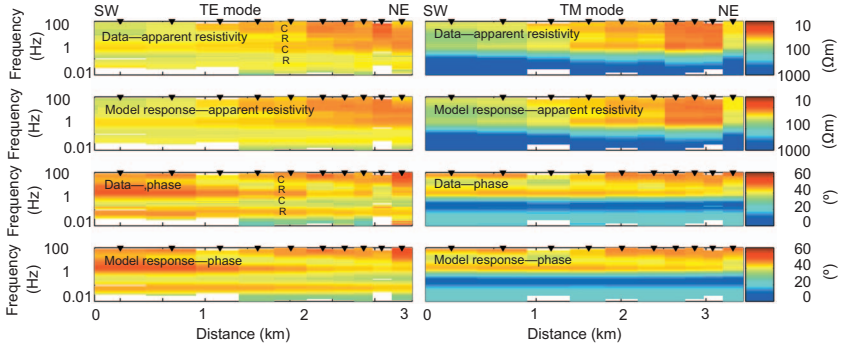

Figure 5. Pseudosection for the Long Shot profile MT data and response of the model in Figure 7. Station locations are denoted by the triangles. The TE mode shows an oscillation of conductive-resistive-conductive-resistive (C-R-C-R) across most of the profile. Data were fit with an rms misfit of 0.818 after 195 iterations.

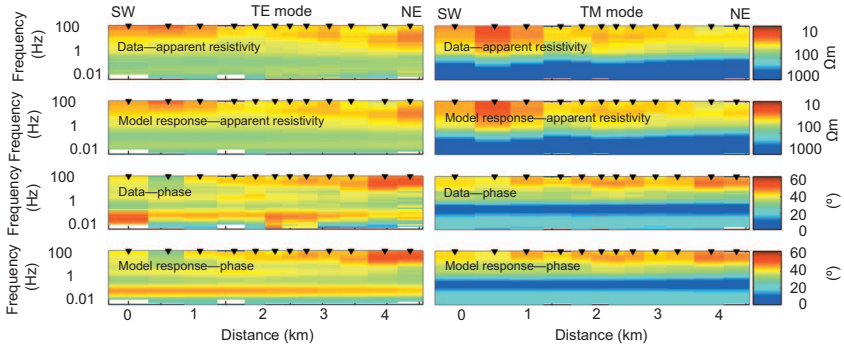

Figure 6. MT data and fit for the Cannikin profile. Data were fit with an rms misfit of 1.211 after 100 iterations.

The Cannikin pseudosection is shown in Figure 6. Note that high-frequency apparent-resistivity values are slightly higher than on the Long Shot profile. The conductive-resistive-conductive-resistive pattern can be seen in the TE-mode apparent resistivity, but it is not as clear as on the Long Shot profile because there is more near-surface variability. This pattern is also observed in the TE phase, especially to the west of Cannikin ground zero. MT data are sometimes affected by static shifts that are the result of small-scale, near-surface structures that spatially alias the MT data (Jones, 1988). Significant static shifts were not observed in the Amchitka Island data set.

MT inversion

To interpret the MT data, the frequency-domain MT data must be converted into a model of subsurface resistivity as a function of true depth. The dimensionality analysis showed that a 2D approach is appropriate, and the inversion algorithm of Rodi and Mackie (2001) was used. The inverse problem of MT is nonunique, which means that if a solution can be found, then an infinite number of models can be found that also fit the data (Parker, 1994). Thus, additional constraints must be applied to the resistivity model to give a unique solution. This process of constraining the solution is termed regularization (Tikhonov and Arsenin, 1979) and generally requires the model to be spatially smooth and/or close to a starting model. Interpretation of MT data from a coastal environment requires that the low resistivity of the seawater is correctly modeled, because seawater is a strong conductor.

A seawater resistivity of 0.3 Ωm was assumed for both the Bering Sea and the Pacific Ocean and a starting resistivity model was developed with a 100-Ωm resistivity seafloor and simplified bathymetry. Two methods were used to include the conductive ocean in the inversion. In the first, the resistivity of the seawater and underlying seafloor

was fixed during the inversion process. This method was found to be unstable and resulted in a spatially rough resistivity model beneath the island. Instability occurs because any inaccuracy in seawater depth cannot be overcome by extending the seawater conductor to depth, and the inversion placed artificial conductors beneath the island. A more satisfactory approach was to use a softer constraint that allowed the regularization to find the smoothest model compared to the starting model. The Long Shot inversion model shown in Figure 7 used data in the frequency band 300–0.001 Hz, with error floors for apparent resistivity and phase of 20% and 4%, respectively. The inversion automatically estimated the static-shift coefficients, but these were small. Figure 5 shows the measured MT data, and the predicted apparent resistivity and phase. These two quantities are very similar, indicating that the measured MT data are well fit. The statistical fit of the data can be measured by the root-mean-square (rms) misfit. A statistically ideal fit would be close to unity, but a value in the range 0.5–1.5 is acceptable. The Long Shot model has an rms misfit of 0.818 and was obtained after 195 iterations.

A profile of resistivity as a function of depth at the Long Shot ground zero is shown in Figure 8b (thick curve). From 0 to 700 m, the resistivity increases, likely because of a freshwater layer with decreasing porosity. From 700 to 1500 m, the resistivity decreases as the salinity increases. Below 1500 m, the saltwater layer is encountered, and a decrease in porosity causes an increase in resistivity. Note that the TZ is observed as the zone where resistivity decreases with depth (Figure 7), and the top of the saltwater layer is located at the depth where resistivity begins to increase again (Figure 1). Many permutations of the inversion control and regularization parameters were investigated to ensure that the final resistivity model did not depend on a particular choice of parameters. The parameter τ controls the balance between fitting the MT data and regularizing the resistivity model. A high value of τ produces a resistivity model that has a poorer fit to the measured MT data, but is spatially smooth. A small value of τ will give a better fit to the MT data, but the model may be rough and contain artifacts. The parameter α controls the balance between horizontal and vertical smoothness of the resistivity model. A value of $\alpha > 1$ produces a model with horizontal layering, while a value of $\alpha < 1$ produces vertical features.

A set of nine inversions that included all combinations of $\alpha = [0.3, 1, 3]$ and $\tau = [1, 3, 10]$ was undertaken (Figure 8), and it can be seen that only small changes are produced in the final resistivity model. The basic pattern of low-high-low-high resistivity was observed in all nine models and shows that the Long Shot inversion model is relatively robust. Other inversion parameters were varied and, in the majority of cases, the same basic resistivity model was obtained. This included using several techniques for estimating static-shift coefficients, changing the value used for the resistivity of the ocean, and altering the frequency range of MT data inverted. The inversion algorithm of Siripunvaraporn and Egbert (2000) produced resistivity models similar to those in Figure 7. The coordinate system used in the 2D inversion was also varied and showed that the model is insensitive to changes in the rotation angle of 5°–10° (Figure 8). The model resolution was also investigated by inverting synthetic MT data (Unsworth et al., 2005).

3D MT forward modeling

There are several strong indicators that the Amchitka Island MT data are 2D above a frequency of 0.1 Hz. These include the dimensionality analysis, the low rms misfits achieved by the 2D inversions, and the similarity of the three inversion models, which show that major changes in resistivity do not occur along the island. Despite these indications, it is important to consider if 3D coastline effects are in-

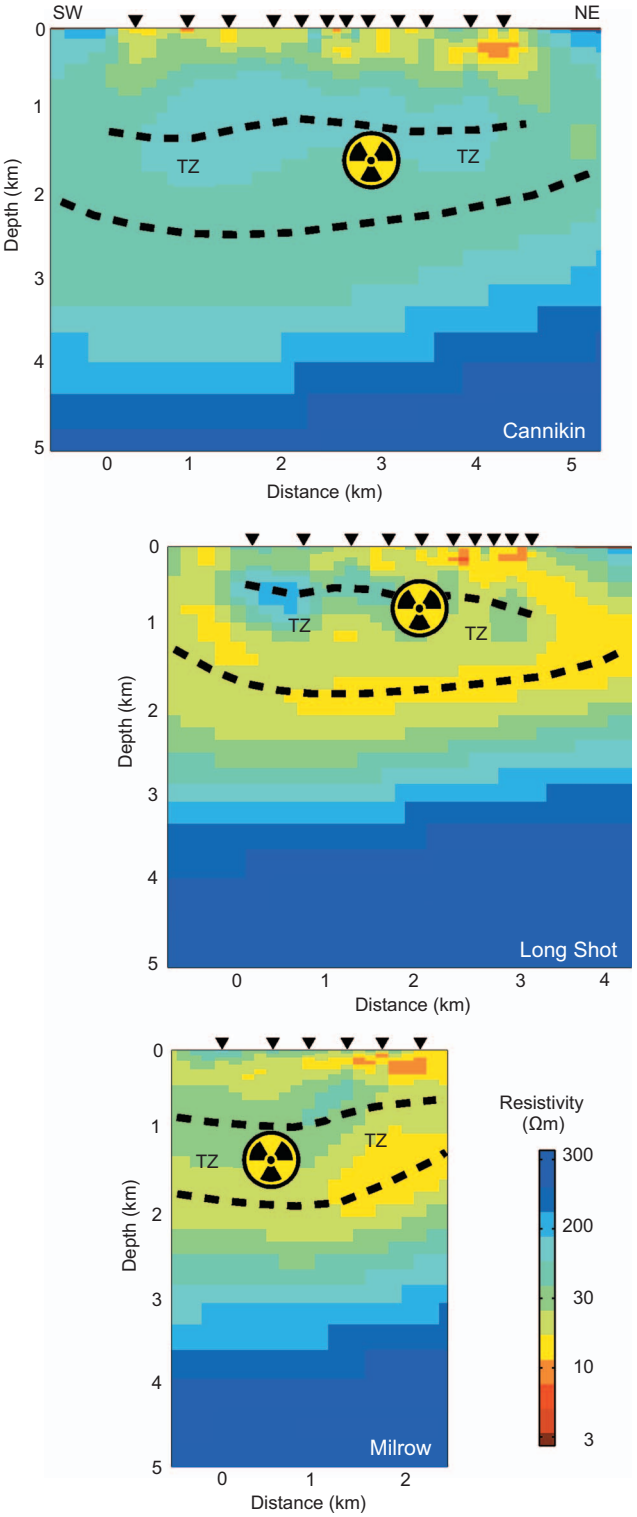

Figure 7. Inversion models for Long Shot, Milrow, and Cannikin profiles. Radiation symbols show the locations of explosions. The dashed lines denote the inferred location of the TZ, defined by the downward decrease in resistivity. Trade-off parameter $\tau = 3$; vertical to horizontal smoothness control parameter $\alpha = 1$.

fluencing the onshore MT data. While the bathymetry is approximately 2D, the finite length of the island must be considered. A set of 3D resistivity models were generated using regional bathymetry data (Figure 9). Forward MT responses were computed using the algorithm of Mackie et al. (1994). Model 1 represents the actual bathymetry around Amchitka Island, with a quasi-layered structure based on Figure 7. In model 2, the island is extended east-west, and in model 3, it is shortened. These changes produce a significant effect on the predicted MT data at frequencies below 0.1 Hz. Since the shallow structure produces responses in the 300–0.1-Hz frequency band, it is unlikely that 3D effects are influencing the models in Figure 7. A range of other 3D models were investigated and gave essentially the same result. The analysis presented in this section has shown that the 2D inversion models for each profile can be considered robust.

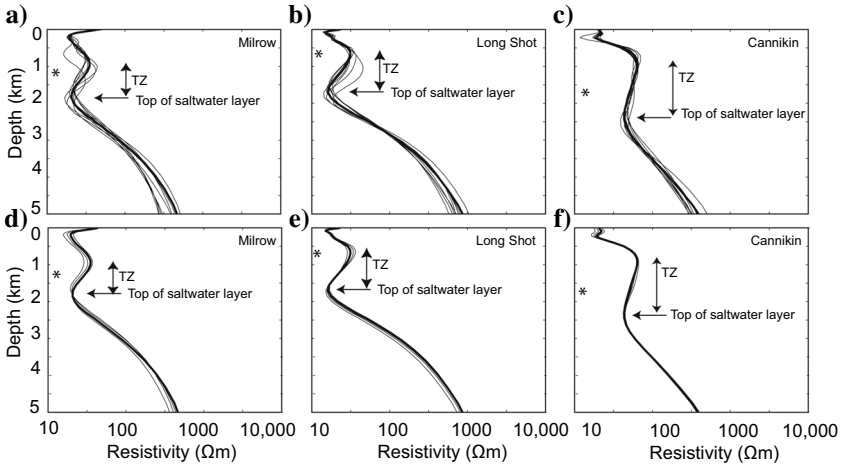

Figure 8. (a-c) Variation of resistivity with depth for a set of nine inversion models with different combinations of inversion-control parameters. The models are shown at ground zero for each profile and use $\alpha = [0.3, 1, 3]$ and $\tau = [1, 3, 10]$. The thick black profile denotes the inversion model for $\alpha = 1$ and $\tau = 3$. Asterisks denote the depths of the explosions. TZ=transition zone. (d-f) Resistivity versus depth as the strike angle is varied. All inversions used $\alpha = 1$ and $\tau = 3$. The thick curve is for the preferred value of N55°W. Other rotation angles are N50°W, N60°W, and N65°W. All inversions are solved directly for static-shift coefficients.

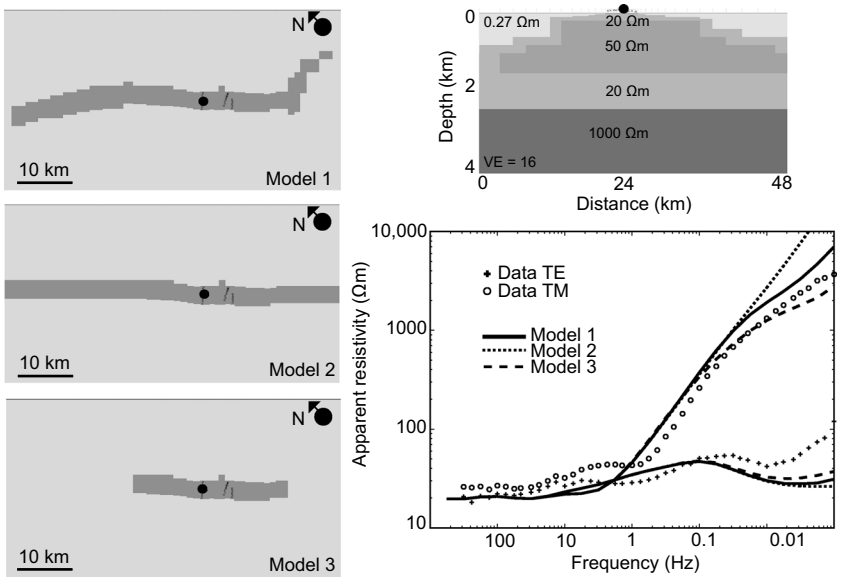

Figure 9. Summary of 3D MT modeling to study the effect of the coastline. The synthetic MT responses are shown at the location denoted by the black circle.

INTERPRETATION

Comparison with well logs

The resistivity models derived from the MT data were compared with well logs described by U. S. Army Corps of Engineers (1965). MT images subsurface resistivity from surface measurements and detects relatively large-scale features. In contrast, the well-log measurement is made within the borehole, much closer to the target, and smaller-scale variations in electric resistivity can be detected. Figure 10a shows the well-log comparison at the Milrow ground zero. The well-log data have been spatially smoothed to allow a more objective comparison. Good agreement is observed between the well logs and the resistivity models, with a steady increase in resistivity from 20 to 40 Ωm. The log for EH-3 is shown in Figure 10b and was measured in the borehole closest to the MT station at Long Shot. This well, plus others not shown, all show a decrease in resistivity from the surface to a value of approximately 10–20 Ωm at a depth of 200–300 m, followed by a steady increase in resistivity from 200- to 800-m depth. This basic pattern is also observed in the resistivity-depth profile derived from the MT measurements. However, the agreement is not as close as observed on the Milrow and Cannikin profiles. Figure 10c shows a comparison of MT-derived resistivity and well-log information for the Cannikin location. Good agreement is observed between the two independent measurements of subsurface resistivity. In the upper 400 m, the resistivity is around 20 Ωm, and this increases to 100–200 Ωm below 600 m. This comparison verifies that subsurface resistivity values are being correctly imaged with the MT data. No major shifts in resistivity have resulted from the proximity to the low-resistivity ocean.

Porosity and salinity at Long Shot and Milrow ground zeros

The models for Long Shot and Milrow show a layered resistivity structure (Figure 7), which can be qualitatively interpreted as outlined in Table 1. Figure 11a shows the salinity (total dissolved solids [TDS]) values from well UAe-2 at Milrow. The uppermost data point is at 400-m depth, and a linear decrease is assumed between this point and the surface. Below 1500 m, the TDS value for seawater is used. The resistivity of the groundwater (ρ_w) was then computed using the empirical relationship of Block (2001). This assumes that the resistivity of the water (in Ωm) is given by $\rho_w = 4.5\ (\mathrm{TDS})^{-0.85}$, where TDS is the amount of total dissolved solids in g/l. As the salinity rises, the resistivity of the water decreases (Figure 11a-11b). The next stage of the analysis is to determine the porosity that is required to give agreement between the resistivity imaged with the MT

data and that predicted by the salinity variation in Figure 11b. In this study, Archie's Law was used to relate the resistivity of a completely saturated rock (ρ_o), the porosity (Φ), and pore-fluid resistivity (ρ_w). Archie (1942) showed that

$$\frac{\rho_o}{\rho_w} = F = \phi^{-m}, \quad (1)$$

where the cementation factor m generally lies between 1.1 and 2.5, and F is the formation factor. The case $m = 1$ corresponds to fluid distributed in cracks, while $m \geq 2$ corresponds to fluid distributed in poorly connected pores and is typically found in carbonates. A value of $m = 1.5$ represents an intermediate case and was used as the preferred value for the expected lithology. Figure 11c shows the computed porosity. The porosity inferred with $m = 1.5$ is 30% at the surface, decreasing to 2% at a depth of 3000 m. The porosity values obtained for Milrow are similar to those reported by Giles et al. (1998), as shown in Figure 12b. Most of these studies report an exponential decrease in porosity with depth (Rubey and Hubbert, 1959). These porosity estimates are in agreement with values of 10%–20% for core in the upper 2 km recovered from pretest drilling (Hassan et al., 2002).

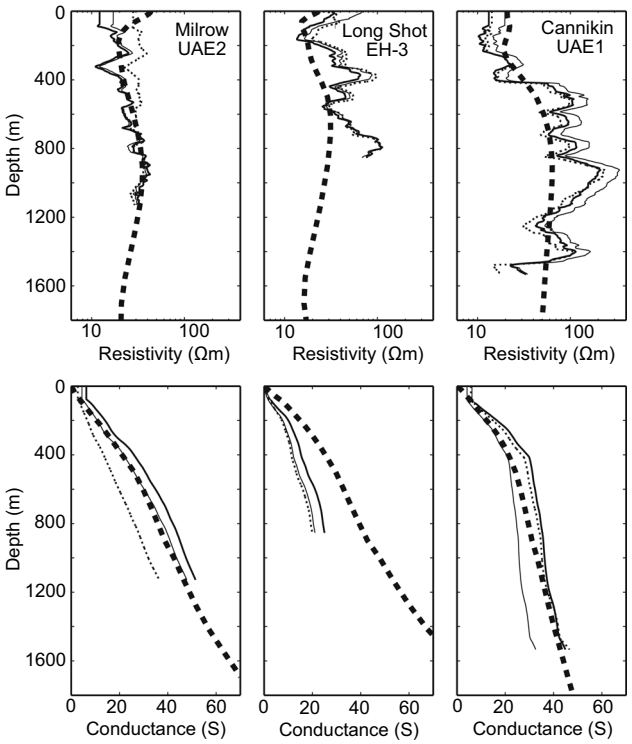

Figure 10. Comparison of the resistivity model (thick dashed line) with the smoothed electric well-log data. The three well-log curves in each well were obtained with different logging tools. Thick continuous = short normal log; thin continuous = long normal log; thin dotted line = lateral log. The lower row shows the conductance integrated with respect to depth.

Table 1. Summary of layers in the hydrogeology model for Milrow.

Layer 1	0–700 m	Increasing resistivity, freshwater, decreasing porosity
Layer 2	700–1500 m	Decreasing resistivity, transition zone, increasing salinity
Layer 3	Below 1500 m	Increasing resistivity, saltwater, constant salinity, and decreasing porosity

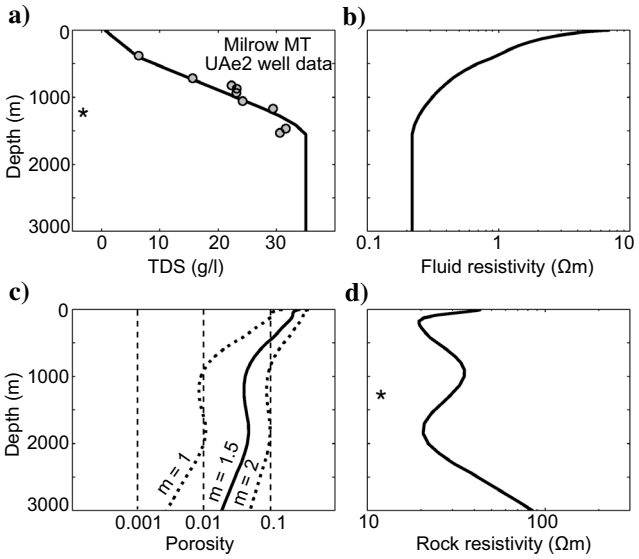

Figure 11. Hydrogeology for Milrow ground zero. (a) Salinity (TDS) at the nearby UAe-2 well (circles). The line denotes a simplified form. (b) Resistivity of the pore fluid derived from (a). (c) Effective porosity required to give agreement between bulk resistivity and that determined by the MT data. Computation uses Archie's Law with exponents m=1, 1.5, and 2. (d) Bulk resistivity from the MT data inversion used as a constraint for (c). The asterisk (*) denotes the depth of the explosion.

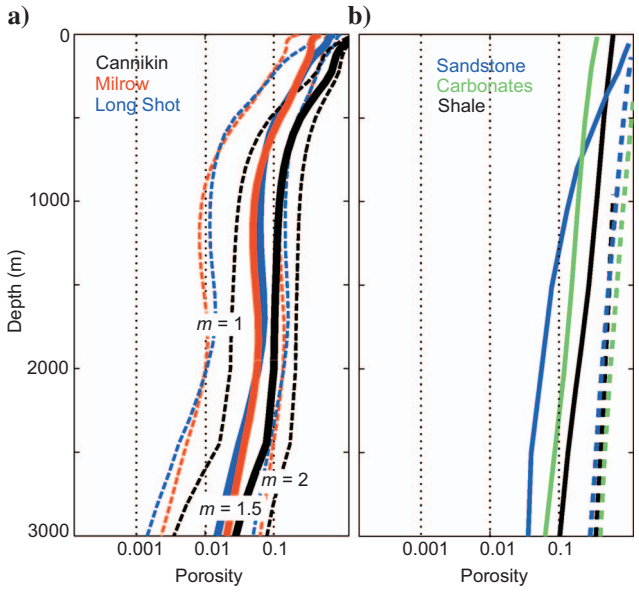

Figure 12. (a) Comparison of effective porosity at the three ground zeros. Note that despite differing values of TDS, the porosities for m = 1.5 are quite similar at Long Shot, Milrow, and Cannikin. (b) Porosities reported by Giles et al. (1998) for carbonates, sandstone, and shale. Solid line denotes lower bound, and the dashed line denotes the upper bound.

Note that measurements made on core give values of total porosity, while those determined from geophysical measurements will be closer to effective porosity; it is expected that the effective porosities measured with MT are less than those made on core. The porosity calculations were repeated with other equations relating salinity and porosity to bulk resistivity, and similar results were obtained (Schilling et al., 1997; Meju, 2000). The top of the TZ is located at a depth of 900 m, where the resistivity begins to decrease. Figure 8 indicates this depth could be in the range 800–1100 m. The base of the TZ is expressed by the depth at which the resistivity increases with depth, where the salinity has reached the seawater value and cannot increase any more. Decreasing porosity below this depth causes a rise in resistivity. Thus, the MT data show that the base of the TZ occurs at a depth of 1700 m at Milrow (Figure 11). Figure 8 indicates that the TZ base is in the range 1500–2100 m. A similar analysis for Long Shot showed a similar porosity-depth variation (Figure 13). Deep well-log information was not available, so salinity data from Milrow (UAe-2) were used, and TZ depths are listed in Table 2.

In summary, realistic values of porosity can explain the observed subsurface resistivities. The MT study confirms the hydrogeologic evidence that both Long Shot and Milrow explosions were detonated toward the upper edge of the TZ. It must be stressed that a limitation of these calculations is that borehole measurements were made prior to the nuclear explosions, while the geophysical measurements were made afterward. If the explosions caused significant changes in subsurface porosity and salinity, then this will influence the calculations.

Porosity and salinity at the Cannikin ground zero

The resistivity models for Cannikin show a layered structure in the upper 4000 m of the subsurface. While the relative depth variations are similar to those observed in the Long Shot and Milrow areas, the absolute resistivity values are higher (Figure 14). This change in absolute-resistivity values is observed in both the MT models and resistivity logs. Salinities at Cannikin are significantly lower than in the Long Shot and Milrow areas, and at a depth of 1500 m in the Milrow shaft, a salinity of 30 g/l was observed in UAe-2 (Beteem et al., 1971). In contrast, at the base of the Cannikin shaft, the reported salinity was 3 g/l (UAe-1). Given the higher elevation of Amchitka Island on the Cannikin profile, it would be expected that the freshwater/saltwater interface would be at a greater depth than in the Long Shot and Milrow areas. Assuming a static groundwater regime and a water table at height h above sea level, buoyancy calculations require that the interface is at a depth of $z = 40h$ below sea level (Ghyben-Herzberg formula, Freeze and Cherry, 1979). On Amchitka Island, the water table is at the surface, and the equation predicts depths of 1800–2200 m and 2800–3200 m in the Long Shot-Milrow and Cannikin areas, respectively, consistent with the depths determined from the MT data. The Ghyben-Herzberg formula also predicts a lens-shaped zone of freshwater, as imaged in Figure 7. It is important to determine what combinations of salinity and porosity are consistent with resistivity models derived from the MT data. The first stage of analysis for Cannikin was to assume that the salinity (TDS) values measured in well UAe-1 for

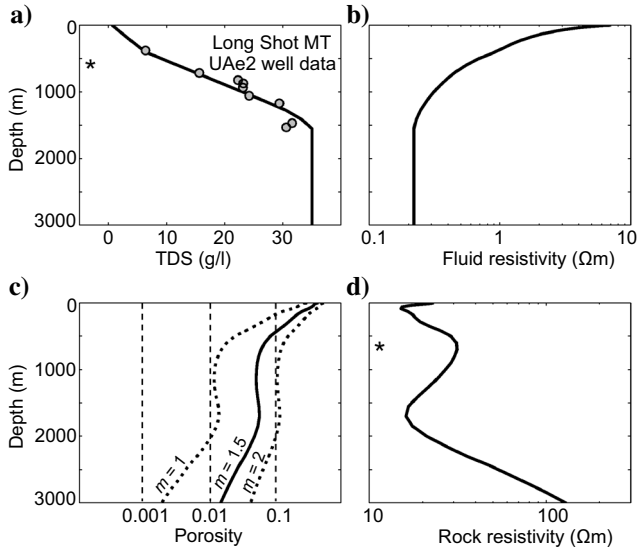

Figure 13. Hydrogeology for Long Shot ground zero. (a) Salinity (TDS) at the nearby Milrow UAe-2 well (circles). Line denotes a simplified form. (b) Resistivity of the pore fluid derived from (a) using the empirical equation of Block (2001). (c) Effective porosity required by the MT data. Computation uses Archie's Law with exponents m = 1, 1.5, and 2. (d) Bulk resistivity from MT data inversion used as a constraint for (c). The asterisk (*) denotes the depth of the explosion.

Table 2. Depth of TZ at the location of each nuclear explosion. For the top and base of the TZ, the preferred value and possible range are listed.

	Shot depth (m)	Top of TZ (m)	Possible range (m)	Base of TZ (m)	Possible range (m)
Milrow	1200	900	800–1100	1700	1500–2100
Long Shot	700	600	500–1000	1700	1500–2000
Cannikin	1700	900	800–1000	2500	2000–2700

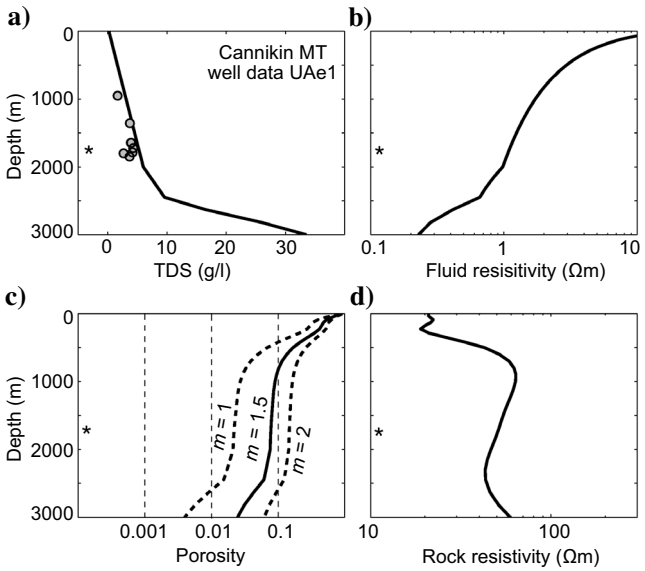

Figure 14. Hydrogeology for Cannikin, showing the same quantities as Figure 13. Note that salinities in well UAe-1 (a) are lower than observed at a similar depth for Milrow. Below the base of the emplacement shaft, the salinity is assumed to rise to the seawater value of 35 g/l. The asterisk (*) denotes the depth of the explosion.

Cannikin are reliable. These TDS values are low, and it has been speculated that they reflect mixing of drilling fluids with the groundwater (Fenske, 1972). The MT data collected in this project provide a way of evaluating these TDS data (Figure 14). Below the bottom of the shaft, a linear increase of salinity to seawater values was assumed. The computed porosity is similar to that at Long Shot and Milrow, and decreases from surface values of 30% to 3% at 3000-m depth.

It is possible that the Cannikin salinity (TDS) data are unreliable, since the values at the base of the shaft are significantly below those expected for seawater. To test this hypothesis, a second calculation was performed. This assumed that the porosity-depth profile obtained for Milrow is also valid for Cannikin. The computation used $m = 1.5$ and showed that an increase in salinity below 2000 m is required to give agreement with the resistivity model derived from the MT data, indicating the presence of the saltwater layer. A simple exponential decay of porosity with depth gave a similar result (Figure 15). This analysis suggests that the reported salinity data in well UAe-1 are consistent with the MT data, assuming a similar porosity-depth variation to that in the Milrow-Long Shot areas. This indicates that the Cannikin cavity is located in the TZ. Note that the transition from fresh to saltwater is indicated by the decrease in resistivity at depth in each model in Figure 7. In the Cannikin model, this occurs at a greater depth than for Milrow and Long Shot. At the greater depth of the Cannikin explosion, the porosity is lower, and the relative decrease in resistivity is smaller. It is possible that the detonation caused significant changes in subsurface structure. The formation of both Cannikin Lake and a chimney has shifted the TZ downward from its location before the explosion.

DISCUSSION

The porosity values at Cannikin are slightly higher than at Milrow and Long Shot, but show a similar trend (Figure 12a). Given the fact that the TDS values for Cannikin and Milrow-Long Shot were quite different, this result suggests that the computational approach is valid, as similar geological structures and porosities are expected in these two parts of the island. It should also be stressed that the porosities computed in this analysis are effective porosities. Many rocks contain dual-porosity systems with fluids in both networks of fractures and isolated pores within the matrix. The MT exploration method uses natural electric currents to image subsurface resistivity, which is dominated by the porosity and interconnection of fluids. This effectively measures the amount of interconnected pore space and is expressed as the m value in Archie's Law. An additional perspective on the porosity values can be obtained by comparison with other studies of porosity-depth variations. Giles et al. (1998) compile a number of data sets for varying lithologies. Note that the porosities inferred for Amchitka Island, with $m = 1.5$, are low compared to the data of Giles et al. (1998), but within the range of observed values. Is it reasonable for the porosities to be systematically higher at Cannikin than at Milrow? The geological setting is essentially the same at the two locations, so that is unlikely to be the explanation. The effect of the explosion would be to increase porosity through fracturing. If the enhanced porosity at Cannikin is the result of the explosion, then a low-resistivity zone should be centered on the shot location. In contrast, the resistivity values at Cannikin are higher across the entire profile. Additionally, an increase in porosity would also have resulted from the 1-megaton Milrow test.

Shallow faults can be observed by their influence on the near-surface resistivity, since they act as barriers to shallow groundwater flow or as conduits of enhanced permeability (Caine et al., 1996). These effects are not observed on Amchitka Island, where the resistivity models are spatially smooth. Another reason for the apparent absence of fault-induced resistivity variations in the models shown in Figure 7 is that most of the faults mapped on Amchitka Island are essentially parallel to the MT profiles. Do the resistivity models in Figure 7 show evidence for features produced by the underground nuclear explosions? A fundamental limitation in answering these questions is that MT profiles were not collected in regions unaffected by the underground nuclear explosions. While each MT profile shows a predominantly layered structure, there are some lateral variations, which are likely because of heterogeneity within the layers, but the nonuniform station spacing can also have some effect. Several features can be seen that may be related to the alteration of the subsurface, especially for the Cannikin profile. These include low-resistivity values in the upper 500 m of the eastern part of the Cannikin line. In this area, the profile crosses the collapse area, and the surface is highly fractured, a situation that would lower the electrical resistivity. There is also a hint in Figure 7 that in the high-resistivity layer at 1000–2000-m depth at Cannikin there is a reduced resistivity coincident with the shot cavity and collapse chimney. However, the station spacing does not allow this feature to be resolved with confidence.

The salinity distribution and porosities defined by the geophysical data are being used as a constraint in modeling the groundwater flow. This uses the FEFLOW algorithm of Diersch (2002) to determine steady-state flow patterns. A homogeneous and isotropic hydraulic conductivity was used to study groundwater flow from the Long Shot cavity. Figure 16a and b shows how the depth of the TZ varies as the hydraulic conductivity and surface recharge were varied. Using the TZ depths defined from the MT, it can be seen that only a subset of these parameters are in agreement with the geophysical obser-

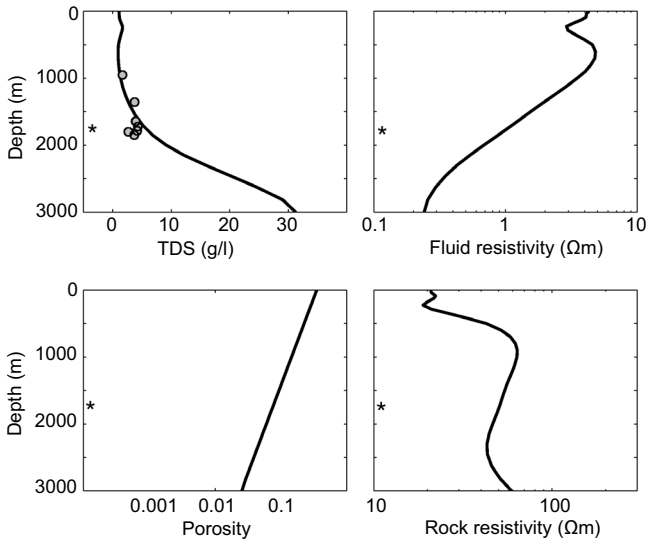

Figure 15. Hydrogeology at the Cannikin ground zero. An exponential porosity depth variation was assumed, and the salinity required to reproduce the variation of resistivity with depth was computed. Note again that a significant increase in salinity is predicted below the depth of the shot cavity. The asterisk (*) denotes the depth of the explosion.

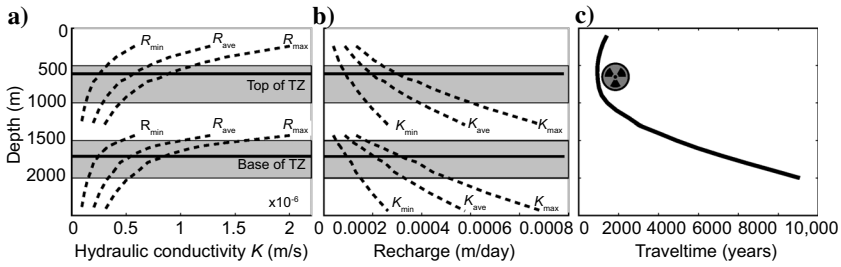

Figure 16. (a) Depth of TZ as a function of hydraulic conductivity (K) for three values of recharge from precipitation (R). The shaded region shows the top and bottom of the TZ as defined by the MT data. $R_{max} = 3.1 \times 10^{-4}$ m/day; $R_{ave} = 2.0 \times 10^{-4}$ m/day; $R_{min} = 9.1 \times 10^{-5}$ m/day. (b) Depth of TZ as a function of recharge for three values of hydraulic conductivity. $K_{max} = 8.5 \times 10^{-7}$ m/s; $R_{ave} = 5.5 \times 10^{-7}$ m/s; $K_{min} = 2.5 \times 10^{-7}$ m/s. (c) Groundwater traveltime to the Bering Sea as a function of explosion depth for a groundwater model of the Long Shot profile on Amchitka Island.

vations. These models were then used to compute transit times from the explosion site to the seafloor. With a recharge value of $R = 3.1 \times 10^{-4}$ m/day and a hydraulic conductivity of $K = 8.5 \times 10^{-7}$ m/s, the TZ occurs between depths of 640 and 1700 m, in agreement with the MT models. The traveltimes for this scenario are illustrated in Figure 16c. An increase in transit time from 900 to 7100 years occurs across the TZ, because flow is slower in the saltwater layer than the freshwater layer. A complete description of the groundwater modeling with geophysical constraints is in progress (A. M. Wagner, D. Barnes, M. J. Unsworth, and D. Kosson, personal communication, 2006).

CONCLUSIONS

MT data collected on Amchitka Island have constrained the depth of the transition from fresh to saltwater beneath Amchitka Island and imply that the cavities created by the three nuclear explosions are located within the TZ. The relatively low salinity data measured in UAe-1 prior to the Cannikin test are consistent with the MT data. Inferred effective porosities are around 30%–40% at the surface, decreasing to 2%–3% at 3000 m. These values are higher than those assumed in several hydrogeologic models, thus giving longer transit times from the explosion to the marine environment. No evidence was found for shallow faults influencing the groundwater flow. Hydrogeologic modeling constrained by these depths suggest that radionuclides from Long Shot explosion could reach the seafloor in 500–1000 years.

ACKNOWLEDGMENTS

This report was prepared with the support of the U. S. Department of Energy, under award no. DE-FG26-00NT40938 to the Institute for Responsible Management, Consortium for Risk Evaluation with Stakeholder Participation II. However, any opinions, findings, conclusions, or recommendations expressed herein are those of the authors and do not necessarily reflect the views of the U. S. Department of Energy. The 2004 field work was made possible by the hard work of Chrystal Rae and William Shulba. We thank Dan Volz for his support as expedition manager. Logistical support from B + N Fisheries and the crew of the F/V *Ocean Explorer* is also gratefully acknowledged. Technical support from Phoenix Geophysics resulted in the high-quality MT data. Bathymetry data were provided by Robert Aguirre, Zygmunt Kowalik, and Mark Johnson. The authors acknowledge discussions with Ben Rostron, Carl Mendoza, David Kosson, and Chuck Powers. Comments by Max Meju and two anonymous reviewers improved this paper.

REFERENCES

Archie, G. E., 1942, The electrical resistivity log as an aid in determining some reservoir characteristics: Transactions of the American Institute of Mineral, Metallic, and Petroleum Engineers, **146**, 54–62.

Beteem, W. A., R. A. Young, C. L. Washington, and L. J. Schroder, 1971, Chemical analyses of water samples collected on Amchitka Island, Alaska: U. S. Army Environmental Command Report USGS-474-135.

Block, D., 2001, Water resistivity atlas of Western Canada: Canadian Society of Petroleum Geologists Annual Convention, Abstracts, 18–22.

Caine, J. S., J. P. Evans, and G. B. Forster, 1996, Fault zone architecture and permeability structure: Geology, **24**, 1025–1028.

Caldwell, T. G., H. M. Bibby, and C. Brown, 2004, The magnetotelluric phase tensor: Geophysical Journal International, **158**, 457–469.

Carr, W. J., and W. D. Quinlivan, 1969, Progress report on the geology of Amchitka Island: U. S. Geological Survey Report USGS-474-44.

Diersch, H.-J. G., 2002, FEFLOW: Finite element subsurface flow and transport simulation system, *in* FEFLOW 5.2 user's manual: WASY, Institute for Water Resources Planning and Systems Research Ltd.

Egbert, G. D., 1997, Robust multiple-station magnetotelluric data processing: Geophysical Journal International, **130**, 475–496.

Egbert, G. D., and J. R. Booker, 1986, Robust estimation of geomagnetic transfer functions: Geophysical Journal of the Royal Astronomical Society, **87**, 173–194.

Fenske, P. R., 1972, Event related hydrology and radionuclide transport at the Cannikin Site, Amchitka Island, Alaska: Desert Research Institute, Center for Water Resources Research Report 45001, NVO-1253-1.

Freeze, R. A., and J. A. Cherry, 1979, Groundwater: Prentice-Hall, Inc.

Gamble, T. D., W. M. Goubau, and J. Clarke, 1979, Magnetotellurics with a remote reference: Geophysics, **44**, 53–68.

Giles, M. R., S. L. Indrelid, and D. James, 1998, Compaction – The great unknown in basin modeling, *in* S. J. Duppenbecker and J. E. Iliffe, eds., Basin modeling: Practice and progress: Geological Society, London, Special Publications, 141, 15–43.

Goldstein, N. E., S. M. Benson, and D. Alumbaugh, 1990, Saline groundwater plume mapping with electromagnetics, *in* S. H. Ward, ed., Geotechnical and environmental geophysics, vol. II: SEG, 17–25.

Hagemeyer, R. T., and M. Stewart, 1990, Resistivity investigation of saltwater intrusion near a major sea-level canal, *in* S. H. Ward, ed., Geotechnical and environmental geophysics, vol. II: SEG, 67–77.

Hassan, A., K. Pohlmann, and J. Chapman, 2002, Modeling groundwater flow and transport of radionuclides at Amchitka Island's underground nuclear tests: Milrow, Long Shot and Cannikin: Nevada Operations Office, National Nuclear Security Administration, U. S. Department of Energy.

Hoekstra, P., and M. W. Blohm, 1990, Case histories of time-domain electromagnetic soundings in environmental geophysics, *in* S. H. Ward, ed., Geotechnical and environmental geophysics, vol. II: SEG, 1–15.

Hubbert, M. K., 1940, The theory of groundwater motion: Journal of Geology, **48**, 785–944.

Jones, A., 1988, Static shift of MT data and its removal in a sedimentary basin environment: Geophysics, **53**, 967–978.

Mackie, L. R., J. T. Smith, and T. R. Madden, 1994, Three-dimensional electromagnetic modeling using finite difference equations: The magnetotelluric example: Radio Science, **29**, 923–935.

McNeill, J. D., 1990, Use of electromagnetic methods for groundwater studies, *in* S. H. Ward, ed., Geotechnical and environmental geophysics, vol. I: SEG, 191–218.

Meju, M. A., 2000, Geoelectrical investigation of old/abandoned, covered landfill sites in urban areas: Model development with a genetic diagnosis approach: Journal of Applied Geophysics, **44**, 115–150.

Parker, R. L., 1994, Geophysical inverse theory: Princeton University Press.

Rodi, W., and R. L. Mackie, 2001, Nonlinear conjugate gradients algorithm for 2-D magnetotelluric inversion: Geophysics, **66**, 174–187.

Rubey, W., and M. K. Hubbert, 1959, Role of fluid pressure in mechanics of overthrust faulting, II: Bulletin of the Geological Society of America, **70**, 167–206.

Schilling, F. R., G. M. Partzsch, H. Brasse, and G. Schwarz, 1997, Partial melting below the magnetic arc in the central Andes deduced from geoelectromagnetic field experiments and laboratory data: Physics of the Earth Planetary Interiors, **103**, 17–31.

Siripunvaraporn, W., and G. D. Egbert, 2000, An efficient data-subspace inversion for two-dimensional magnetotelluric data: Geophysics, **65**, 791–803.

Tikhonov, A. N., and V. Y. Arsenin, 1979, Methods for solving Ill-posed problems: Nauka.

Unsworth, M. J., X. Lu, and M. D. Watts, 2000, CSAMT exploration at Sellafield: Characterization of a potential radioactive waste disposal site: Geophysics, **65**, 1070–1079.

Unsworth, M. J., P. E. Malin, G. D. Egbert and J. R. Booker, 1997, Internal structure of the San Andreas fault zone at Parkfield, California: Geology, **25**, 359–362.

Unsworth, M., W. Soyer, and V. Tuncer, 2005, Magnetotelluric measurements for determining the subsurface salinity and porosity structure of Amchitka Island, Alaska, *in* C. W. Powers et al., eds., Biological and geophysical aspects of potential radionuclide exposure in the Amchitka marine environment: Consortium for Risk Evaluation with Stakeholder Participation, Institute of Responsible Management, http://www.instrm.org/Amchitka_Final_Report/finalreport/chapters/06_Chapter6_F7_26_05.pdf, accessed November 2006.

U. S. Army Corps of Engineers, 1965, Project Long Shot, Amchitka Island, Alaska: Geologic and hydrologic investigations (Phase I): U. S. Army Engineer District, Alaska and U.S. Geological Survey.

Ward, S. H., 1990, Resistivity and induced polarization methods, *in* S. H. Ward, ed., Geotechnical and environmental geophysics: SEG, 147–189.

Wheatcraft, S. W., 1995, Sea water intrusion model of Amchitka Island, Alaska: Nevada Operations Office, U. S. Department of Energy, Report DOE/NV/10845-59.